IOPscience iopscience.iop.org

Home Search Collections Journals About Contact us My IOPscience

Characterization of vapour-transport-equilibrated Yb(/Er):$LiNbO_3$ crystals

This article has been downloaded from IOPscience. Please scroll down to see the full text article.

2004 J. Phys.: Condens. Matter 16 7793

(http://iopscience.iop.org/0953-8984/16/43/019)

View the table of contents for this issue, or go to the journal homepage for more

Download details:
IP Address: 129.252.86.83
The article was downloaded on 27/05/2010 at 18:24

Please note that terms and conditions apply.

INSTITUTE OF PHYSICS PUBLISHING JOURNAL OF PHYSICS: CONDENSED MATTER

J. Phys.: Condens. Matter **16** (2004) 7793–7811 PII: S0953-8984(04)81869-1

Characterization of vapour-transport-equilibrated Yb(/Er):$LiNbO_3$ crystals

De-Long Zhang[1,2], **W H Wong**[1] **and E Y B Pun**[1]

[1] Department of Electronic Engineering, City University of Hong Kong, Kowloon, Hong Kong, People's Republic of China
[2] Department of Opto-electronics Information Engineering, College of Precision Instruments and Opto-electronics Engineering, Tianjin University, Tianjin 300072, People's Republic of China

E-mail: delongzhang@eyou.com

Received 9 June 2004
Published 15 October 2004
Online at stacks.iop.org/JPhysCM/16/7793
doi:10.1088/0953-8984/16/43/019

Abstract

Visible and infrared absorption, Raman scattering, x-ray powder diffraction and scanning electron microscope (SEM) have been used to characterize Er/Yb (0.6 mol%/0.3 mol%) codoped and singly Yb-doped (1.2 mol%) *Z*-cut $LiNbO_3$ crystals that were vapour-transport-equilibrated (VTE) at 1110 and 1120 °C for 100, 120 and 220 h in a Li-rich atmosphere. Optical absorption edge and 153 cm^{-1} E(TO) phonon linewidth have been used to roughly evaluate the composition of the crystals. The results obtained show that the VTE treatment has brought all crystals towards stoichiometric composition. As a relatively strong VTE condition was adopted, the treatment results in the formation of submicron-sized $ErNbO_4$ (+$YbNbO_4$) and $YbNbO_4$ flat polyhedron-like precipitates in the Er/Yb:$LiNbO_3$ and Yb:$LiNbO_3$ crystals, respectively. On the other hand, a relatively weak VTE procedure cannot induce the precipitation of both the singly and doubly doped crystals. The characteristic optical absorptions, characteristic x-ray diffractions, crystalline structure and crystallographic morphology of the $ErNbO_4$ and $YbNbO_4$ precipitates are discussed, summarized and compared with those of singly Er-doped $LiNbO_3$ crystals reported previously. The absorption characteristics of the unprecipitated Er/Yb codoped and singly Yb-doped crystals are also summarized and compared with the case of singly Er doping. An atomic force microscope has been used to further verify the SEM results and to evaluate the roughness of the surface of precipitated crystals. Optical absorption measurement was also carried out on a precipitated Er/Yb codoped crystal with polished surfaces to verify that the precipitates grow not only on the surface of the crystal but also in the bulk.

 © 2004 IOP Publishing Ltd Printed in the UK

1. Introduction

The Er:$LiNbO_3$ crystal is a potential host material for active integrated opto-electronic devices because it combines excellent electro-optic, acousto-optic and nonlinear optical properties of $LiNbO_3$ crystal with laser gain of Er^{3+}. Such an effective combination, together with the possibility of producing a high-quality waveguide of low loss, resulted in the demonstration of a family of Ti:Er:$LiNbO_3$ waveguide lasers (amplifiers) and integrated devices over the past decade [1–9]. Nevertheless, the singly Er-doped material still shows some imperfections. One main drawback is the lower absorption cross-section in the wavelength range of 800–1500 nm, which is suitable for laser diode pumping. This weakness hence limits the pump efficiency. A possible improvement is codoping the material with Yb^{3+}, which acts as a sensitizer of Er^{3+} ion. The sensitization provides several advantages, which include a stronger absorption cross-section, a broader absorption band in the near-infrared region of 880–1050 nm, which can offer the possibility of excitation tuning, as well as the large overlap between Yb^{3+} emission and Er^{3+} absorption that allows an efficient resonant energy transfer from Yb^{3+} ions to Er^{3+} ions [10–14]. In addition, Er/Yb codoping can also realize dual-wavelength lasing in a strip waveguide [15] and simultaneous multi-colour generations in an aperiodically poled nonlinear channel waveguide in terms of the concept of frequency conversion [16].

Recently, the vapour transport equilibration (VTE) technique has been applied to singly Er-doped $LiNbO_3$ [17, 18]. Earlier studies have shown that the nearly stoichiometric Er:$LiNbO_3$ crystal reveals a number of interesting spectral and spectroscopic characteristics in comparison with the congruent material [17–20]. Some of these characteristics are favourable for its application in integrated opto-electronics. On the other hand, as the doping level of erbium is high enough, 2.0 mol% for example, VTE treatment induces the formation of an additional $ErNbO_4$ phase in the crystal, whether the crystal is *X*-cut or *Z*-cut [21–22]. Formation of the additional phase results in interesting phonon vibration, absorption and emission features, including remarkable Raman intensity changes of individual phonons [18], significant absorption features in the 1450–1650 nm region, opacity in the visible region, near transparency at about 1.53 μm [19], substantial weakening of the visible emission arising from the scattering effect of precipitates [20], etc. It is not only of interest but also necessary to investigate the influence of VTE treatment on the Er/Yb codoped crystal. In this work, *Z*-cut Er/Yb codoped $LiNbO_3$ crystals were VTE-treated at different temperatures for different durations. Visible and infrared absorption, Raman scattering, x-ray powder diffraction and scanning electron microscope (SEM) have been used to characterize the optical, structural and morphological features of these VTE Er/Yb codoped crystals in comparison with the corresponding as-grown crystal. For reference, characterizations were also carried out on *Z*-cut singly Yb-doped VTE crystals.

2. Experimental details

2.1. Sample preparation

Z-cut Er/Yb (0.6 mol%/0.3 mol%):$LiNbO_3$ and *Z*-cut Yb (1.2 mol%):$LiNbO_3$, congruently grown by the conventional Czochralski method, were used as the initial materials. The rare-earth doping level given here is the Er^{3+} or Yb^{3+} concentration in the starting melts. A number of thin plates of these crystals with a thickness of less than 1 mm experienced a total of two rounds of the VTE treatment. The first round of VTE experiment (named V1 procedure) was carried out at 1110 °C for 120 h. The second round of treatment (named V2 procedure) was carried out at a higher temperature of 1120 °C for a relatively shorter duration of 100 h.

Both the rounds of experiment used the same Li-rich two-phase powder ($LiNbO_3 + Li_3NbO_4$), prepared by sintering Li_2CO_3 and Nb_2O_5 mixing powder in a molar ratio of 65 : 35. Details of the VTE procedure were described in our earlier report [18]. We obtained totally two and three kinds of VTE samples for Er/Yb codoping and Yb single doping, respectively. Each kind of VTE sample has several pieces that are enough for the subsequent optical absorption, Raman scattering, x-ray powder diffraction and SEM characterizations. A detailed description of these crystals is given in table 1. The footnotes in table 1 specify the VTE conditions employed in this work. In principle, to increase the efficiency of the VTE, fine-polish is usually not performed on the plate prior to the VTE experiment. Nevertheless, to facilitate the subsequent optical, Raman and SEM characterization, two main surfaces of each plate were fine-polished prior to the VTE treatment.

To help in the determination of the precipitation phase generated in the Yb:$LiNbO_3$ crystal, $YbNbO_4$ powder was prepared by thermally calcining a mixture of Yb_2O_3 powder with a purity of 99.9% and Nb_2O_5 powder with a purity of 99.99% in the molar ratio 1 : 1. The calcination was carried out at 1600 °C for 31 h in a bottom loading furnace (BLF18/8).

2.2. Optical absorption

After the VTE procedure(s), all VTE samples were first subjected to optical absorption measurements by using a Perkin–Elmer Lambda-19 UV/VIS/NIR spectrometer. The scanning wavelength range was 280–1700 nm. The scanning step and scanning speed were fixed at 0.5 nm and 120 nm min^{-1}, respectively. The transmission spectra of these VTE crystals in the OH^- absorption region were recorded by using the Perkin–Elmer FTIR Spectrum One system. The scanning range and scanning step were fixed at 3300–3700 cm^{-1} and 1 cm^{-1}, respectively. Each spectrum was obtained as a result of an average on eight scans. Some optical absorption results allow us to preliminarily discriminate some precipitated samples.

2.3. Raman scattering

To evaluate the Li^+ composition in these crystals in terms of the phonon linewidth, the E(TO) Raman spectra of the as-grown and VTE-treated crystals were recorded in the wavenumber range of 50–1000 cm^{-1} by using a Jobin-Yvon T64000 spectrometer, equipped with a CCD detector cooled by liquid nitrogen. The 488 nm line emitted from an INNOVA 705 argon laser was used as the excitation source. The excitation power was fixed at 150 mW. The polarized excitation light was focused on the sample by a 10× objective microscope.

For 3 m symmetry, the Raman tensors are given by

$$A_1(Z): \begin{pmatrix} a & 0 & 0 \\ 0 & a & 0 \\ 0 & 0 & b \end{pmatrix}, \qquad E(Y): \begin{pmatrix} c & 0 & 0 \\ 0 & -c & d \\ 0 & d & 0 \end{pmatrix}, \qquad E(X): \begin{pmatrix} 0 & c & d \\ c & 0 & 0 \\ d & 0 & 0 \end{pmatrix}.$$

The Raman scattering intensity of a polar lattice vibrational mode in a uniaxial crystal, after considering an additional scattering arising from a polarized electric field generated by a longitudinal mode, is given by

$$I = A \left| \sum_{\beta,\alpha,\gamma=X,Y,Z} e_{1\beta} p_{\beta\alpha}(\gamma)[\rho e_\gamma + \sigma e_{q\gamma}] e_{2\alpha} \right|^2, \tag{1}$$

where $e_{1\beta}$ and $e_{2\alpha}$ ($\alpha, \beta = X, Y, Z$) are Cartesian projection components of the unit polarization vector of incident light and scattering lights, respectively; $p_{\beta\alpha}(\gamma)$ ($\gamma = X, Y, Z$) is a component

Table 1. A summary of the preparation conditions of VTE Er/Yb codoped and singly Yb-doped $LiNbO_3$ crystals and their optical and spectral parameters, including optical absorption edge, 153 cm^{-1} E(TO) phonon linewidth, typical absorption peak position and FWHM, and integrated absorption coefficient concerning the $^2F_{7/2} \rightarrow {}^2F_{5/2}$ (Yb^{3+}), $^4I_{15/2} \rightarrow {}^4I_{11/2}$ (Er^{3+}) and $^4I_{15/2} \rightarrow {}^4I_{13/2}$ (Er^{3+}) transitions. The $(Li^+ + RE^{3+})/Nb$ ratio ($RE^{3+} = Er^{3+} + Yb^{3+}$ or Yb^{3+}) in each sample, evaluated from the optical absorption edge or Raman linewidth of the 153 cm^{-1} E(TO) phonon, is also given. Also listed are rough planar dimensions of the $ErNbO_4$ and $YbNbO_4$ precipitates.

	Dopant(s)/doping level/crystal cut						
	Er/Yb codoping/0.6/0.3 mol%/*Z*-cut			Single Yb-doping/1.2 mol%/*Z*-cut			
VTE condition	As-grown	V1	V1 + V2	As-grown	V1	V2	V1 + V2
OAE at 20 cm^{-1} (nm)	320	311	421	320	312.5	428	493
FWHM of 153 cm^{-1} E(TO) phonon (cm^{-1})	11.34	8.31	7.45	12.85	9.05	8.20	7.86
$(Li^+ + RE^{3+})/Nb$ ratio (%) evaluated from OAE	93.8	98.1		93.8	97.5		
$(Li^+ + RE^{3+})/Nb$ ratio (%) evaluated from Raman	93.8	98.0	98.9	93.8	97.7	98.6	99.0
Peak position of typical absorption (nm)	979.5 1530.5	979.7 1530.9	979.9 1531.2	979.2	979.4	979.4	979.6
FWHM of the typical absorption peaks (nm)	3.69 3.36	3.95 3.00	4.95 3.26	3.77	3.77	4.34	4.37
880–1050 nm absorption band area (nm cm^{-1})	61.1	55.1	29.6	178.9	163.7	160.1	131.5
1450–1650 nm absorption band area (nm cm^{-1})	70.0	63.1	67.0				
Precipitation or not	–	Not	Yes	–	Not	Yes	Yes
Length range of precipitates (nm)			200–980			400–1030	
Width range of precipitates (nm)			100–285			250–630	

V1, 1110 °C/120 h, Li_2CO_3:Nb_2O_5 = 65 : 35; V2, 1120 °C/100 h, Li_2CO_3:Nb_2O_5 = 65 : 35.

of the Raman scattering tensor; e_γ is the projection component of the unit vibrational vector of the polar phonon involved; $e_{q\gamma}$ is the projection component of the unit wavevector of the phonon involved. ρ and σ are constants and σ is proportional to the polarized electric field. For a uniaxial crystal, when the wavevector is parallel to the optical axis Z, the recorded A_1 mode is a longitudinally extraordinary phonon A_1(LO) and the recorded E modes include transversely extraordinary and ordinary phonons and are degenerate. In connection with the crystals studied, considering that all the samples are thin Z-plates, a backward-scattering configuration is the more convenient and appropriate choice. In principle, the $Z(YX)\bar{Z}$ or $Z(XY)\bar{Z}$ configuration appears to be an appropriate geometry, because the recorded spectrum is pure E(TO) mode. But the experimental result has shown that the recorded spectrum under such configurations is so weak that it cannot be utilized. Here, we chose the $Z(YY)\bar{Z}$ geometry. Under this configuration, the recorded spectrum is the overlap of the A_1(LO) and E(TO) modes. Nevertheless, the 153 cm^{-1} Raman peak that we are interested in corresponds to the pure E(TO) phonon. The theoretical scattering intensity is $Aa^2(\rho+\sigma)^2$ and $Ac^2\rho^2$ for A_1(LO) and E(TO) modes, respectively.

2.4. X-ray diffraction and SEM experiments

The precipitated samples were further studied by using x-ray powder diffraction to confirm the formation of precipitates in these samples. The generated additional phase, $ErNbO_4$ or $YbNbO_4$, was thus determined. To realize this objective, x-ray powder diffraction measurement was also carried out on the thermally calcined $YbNbO_4$ powder and a Z-cut singly Er-doped (2.0 mol%) $LiNbO_3$ crystal that was VTE-treated simultaneously with the V1 + V2 Er/Yb:$LiNbO_3$ or Yb:$LiNbO_3$ crystals. The x-ray diffraction experiment was accomplished by using a Rigaku x-ray diffractometer equipped with a Cu target. The operated voltage and current of the target were 40 KV and 100 mA, respectively. The 2θ scanning range was 5–90°. The scanning speed and step were 8° min^{-1} and 0.04°, respectively.

Finally, SEM characterization was performed on two V1 + V2 crystals, one codoped and the other Yb-singly doped. Formation of the dominant precipitates, $ErNbO_4$ in the former and $YbNbO_4$ in the latter, has been confirmed by the combined optical absorption and x-ray results. SEM images were taken by using a Philips XL 40 field emission gun (FEG) scanning electron microscope. Due to the low electric conductivity of $LiNbO_3$ crystals, the acceleration voltage was operated at a level as low as 1 kV to degrade the electric charge accumulation to a large extent.

3. Results and discussion

3.1. Optical absorption characteristics

In figures 1, 2 and 3(a), we show the absorption spectra of two VTE-treated Er/Yb codoped crystals in the wavelength range of 300–800, 880–1050 and 1450–1650 nm, respectively. The spectrum of the crystal that experienced the V1 procedure is shown by dash curves and that of the V1 + V2 sample by solid lines. For comparison, the spectra of the as-grown crystal are also shown (dot curves). To facilitate the observation of spectral features, several typical absorption bands or peaks are more clearly shown in the insets. These bands or peaks include bands at 380 and 520 nm and peaks at 980 and 1530 nm, which correspond to the electron transition absorption of Er^{3+} from the ground state $^4I_{15/2}$ to the excited manifolds $^4G_{11/2}$, $^2H_{11/2}$, $^4I_{11/2}$ and $^4I_{13/2}$, respectively. The spectra shown in 880–1050 nm involve the spectral overlap of two different absorption transitions of $^2F_{7/2} \rightarrow {}^2F_{5/2}$ (Yb^{3+}) and $^4I_{15/2} \rightarrow {}^4I_{11/2}$ (Er^{3+}).

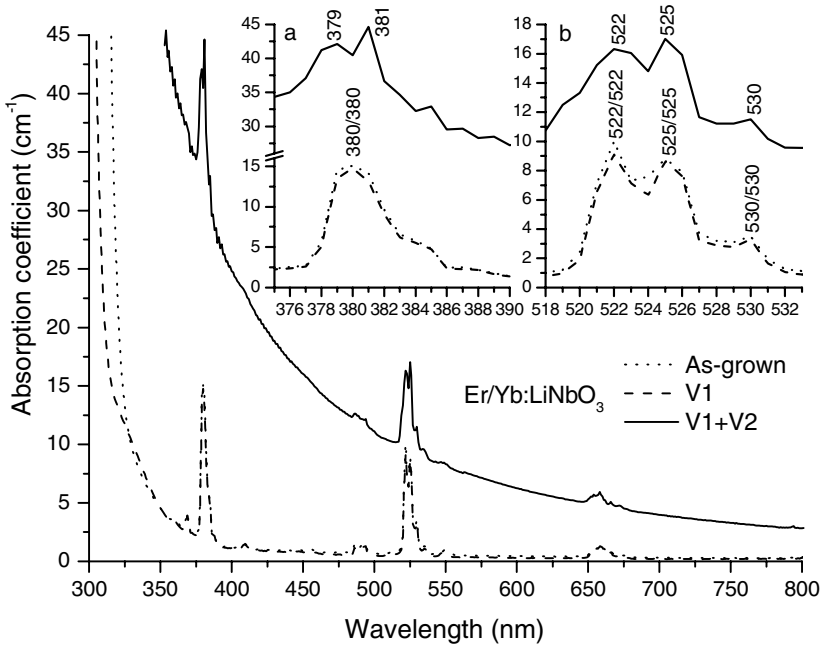

Figure 1. Absorption spectra of as-grown and VTE-treated Er/Yb codoped $LiNbO_3$ crystals in the wavelength range of 300–800 nm. The insets show an expanded view of two main absorption bands near 380 and 530 nm. The dot, dash and solid curves correspond to as-grown, V1 and V1 + V2 crystals, respectively.

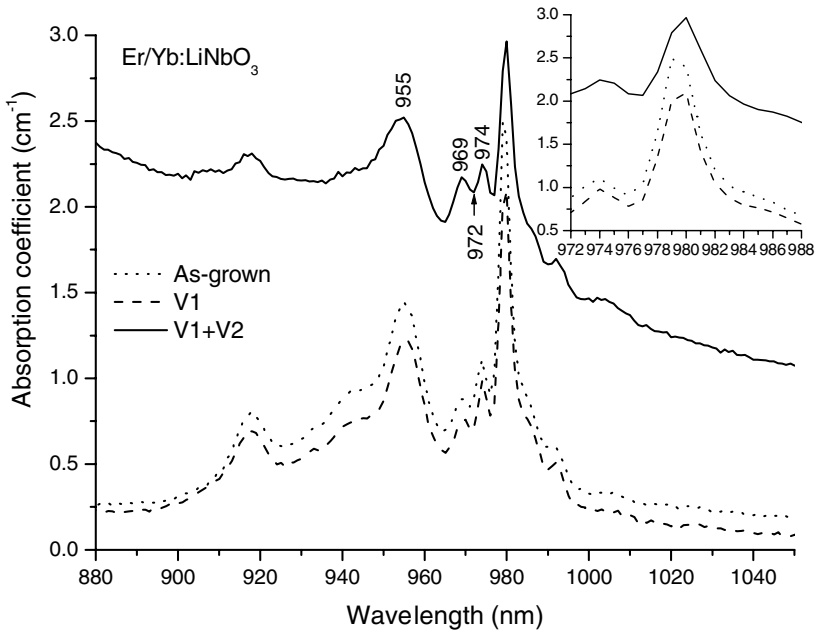

Figure 2. Absorption spectra of the same Er/Yb crystals as in figure1 in the 880–1050 nm region. The inset shows an expanded view of the typical absorption peak near 980 nm.

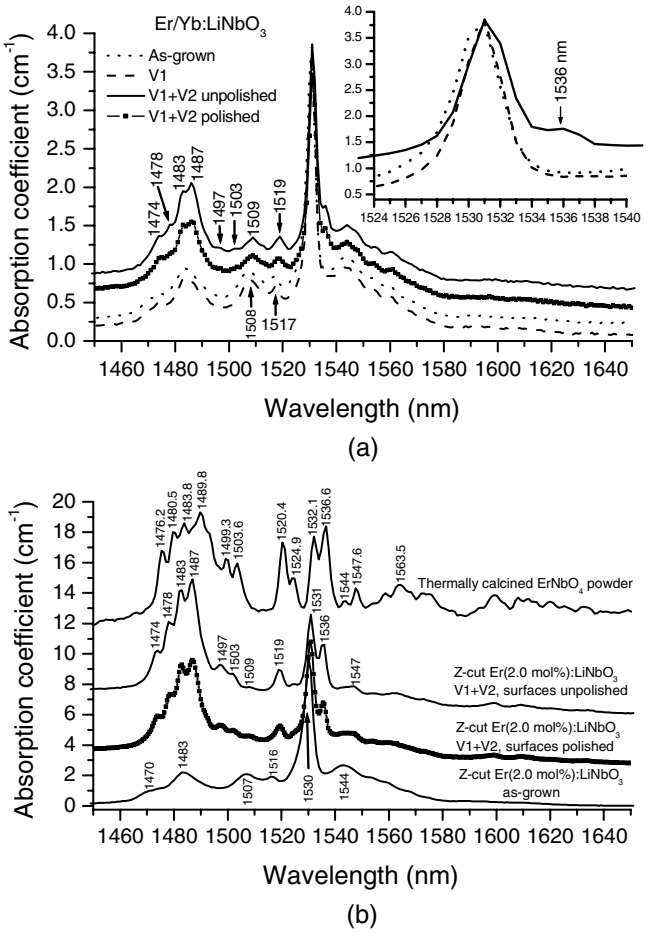

Figure 3. Absorption spectra of Er^{3+} ions in the 1450–1650 nm region. (a) As-grown, V1, V1 + V2 (unpolished after VTE) and V1 + V2 (polished after VTE) Er/Yb:$LiNbO_3$ crystals. The inset shows an expanded view of the typical absorption at 1530 nm. (b) As-grown and (V1 + V2)-treated singly Er-doped (2.0 mol%) $LiNbO_3$ with and without the polished surface, and calcined $ErNbO_4$ powder.

Figures 4 and 5 show the absorption spectra of three VTE-treated and one as-grown Yb:$LiNbO_3$ crystals in the wavelength of 300–800 and 880–1050 nm, respectively. The spectra of the as-grown, V1, V2 and V1 + V2 samples are denoted numerically by dot, dash, dash-dot-dot and solid curves. The inset in figure 5 shows the 980 nm peaks in an expanded view. It should be pointed out that the label 'unpolished' for the spectrum of the V1 + V2 Er/Yb codoped crystal shown in figure 3(a) means that the two surfaces of the crystal employed were not subjected to a fine-polishing process after the VTE procedure and the label 'polished' means that the two surfaces of the crystal were polished after the VTE procedure (similarly in figure 3(b)). In sections 3.1–3.3, the spectra of only the unpolished crystals are discussed, whereas the spectra of the polished crystals will be discussed in section 3.4.

First of all, let us pay attention to the optical absorption edge (OAE) characteristics of these VTE crystals. Usually, the position of the OAE is defined as the wavelength where the absorption coefficient is 15 or 20 cm^{-1}. In this work the OAE data, defined at an absorption

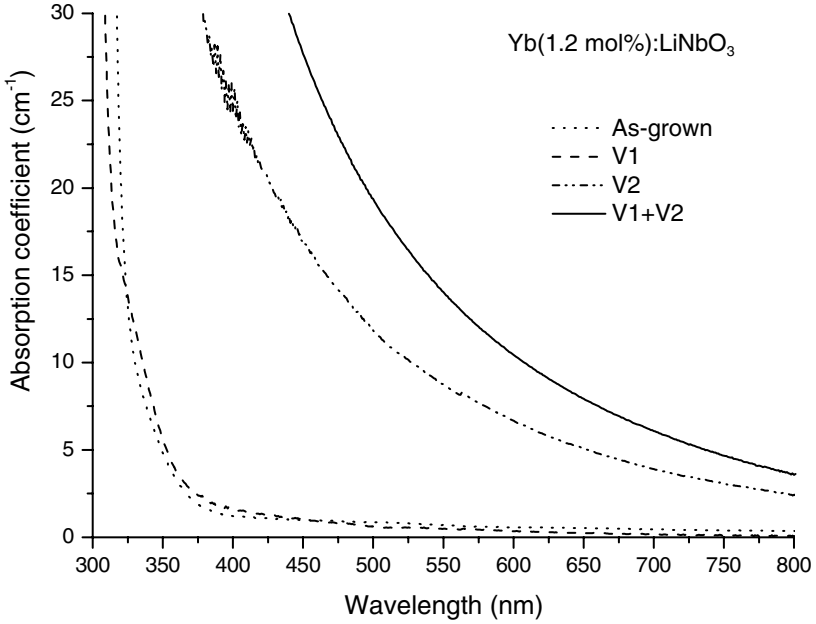

Figure 4. Absorption spectra of as-grown and VTE-treated singly Yb-doped (1.2 mol%) $LiNbO_3$ crystals in the wavelength range of 300–800 nm. The dot, dash, dash-dot-dot and solid curves correspond to as-grown, V1, V2 and V1 + V2 crystals, respectively.

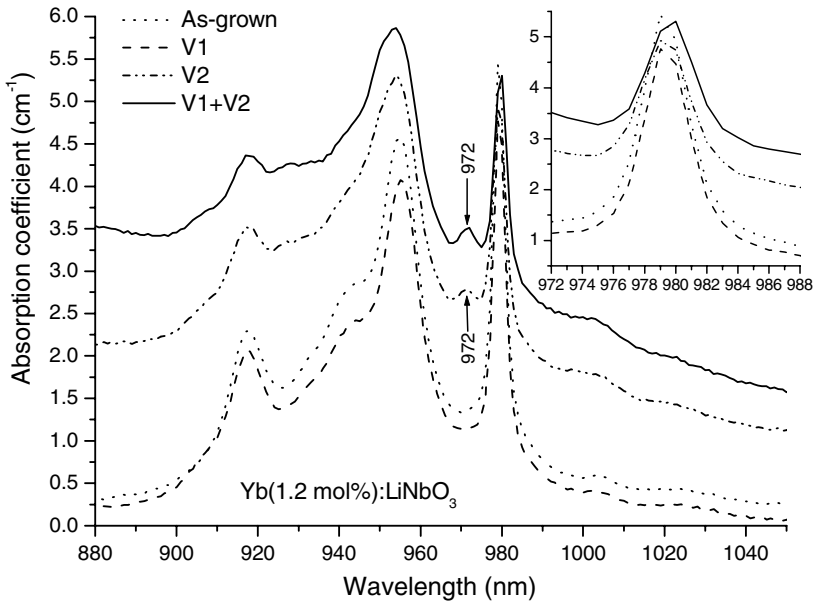

Figure 5. Absorption spectra of the same crystals as those of figure 4 in the wavelength range of 880–1050 nm. The inset shows an expanded view of the typical absorption peak near 980 nm.

coefficient of 20 cm^{-1}, are considered. We note from figures 1 and 4 that the OAEs of the two crystals with the V1 procedure show obvious blueshift as compared with those of the corresponding as-grown ones. Both as-grown samples have the same OAE value of 320 nm as that of the pure $LiNbO_3$ crystal. After the V1 procedure, the OAE moves to 311 and 312.5 nm for the doubly and singly doped samples, respectively. In addition, the V1 procedure also results in very slight reduction of the background absorption as seen by comparing the dash and dot curves of figures 1–5. This result may be doubted due to the possible changes in sample position when replacing the sample. A small tilt of the sample can cause a difference in the reflectivity that could be responsible for the background absorption difference. This doubt can be ruled out because we employed a special sample holder for the optical absorption measurement. The holder can be precisely assembled with the sample support that is fixed at the base of the spectrometer. By employing such a holder, the possibility of sample tilting arising from replacing the sample could be avoided. Moreover, the appearance features of the unprecipitated VTE crystal also support the result. After the VTE treatment, it was found that the unprecipitated crystal becomes more lucid and transparent, because the VTE treatment induces the reduction of intrinsic defects and the lattice has to be nearly perfected.

In contrast to the above two V1-treated crystals, three other VTE crystals, including one Er/Yb:$LiNbO_3$ with the V1 + V2 procedure and two Yb:$LiNbO_3$ crystals with the respective V2 and V1 + V2 procedures, show an obvious opacity characteristic in the visible region. The opacity even extends to the near-infrared region as shown in figures 2, 3(a) and 5. The opacity characteristic is one of the main spectral features that indicate the existence of additional crystalline phase(s). In other words, some precipitates may be induced in the three opaque crystals. The opacity is not the result of absorption of the generated precipitates but from their Rayleigh scattering, which is stronger for a light with a shorter wavelength and weaker for that with a longer wavelength. Due to the opacity, the OAE of these VTE crystals shows a large redshift relative to that of the as-grown crystal, as shown in figures 1 and 4. Table 1 lists the OAE values of all VTE and as-grown crystals studied.

A VTE-induced OAE blueshift and very slight reduction of the background absorption in the two V1 crystals or VTE-induced precipitation in the V2 and V1 + V2 crystals are the main spectral features of the increase in Li content of the crystals. According to Wohlecke *et al* [23], the OAE for the absorption coefficient of 20 cm^{-1} can be expressed as

$$\lambda_{20} = 320.4 - 1.829x - 5.485x^2, \tag{2}$$

where x represents the deviation from the congruent composition (48.38 mol%) in mol%. It should be pointed out that this expression is valid for the light being polarized parallel to and propagating perpendicular to the optical axis Z, i.e. valid for the π-polarized spectrum. For our Z-cut crystals, however, the recorded spectra are α-polarized. The above experiential expression is therefore not exactly suitable for our spectra. However, our experimental results have shown that, under the unpolarized absorption measurement, both as-grown Er/Yb codoped and as-grown Yb singly-doped crystals, as well as other as-grown singly Er-doped $LiNbO_3$ crystals with different doping levels, have almost the same OAE at 20 cm^{-1}, 320 nm, whether the crystal is Z-, X- or Y-cut. This OAE value is also the same as that of the pure crystal under the π-polarization [23]. Thus, equation (2) may be used for a rough evaluation of the composition in the crystal. The $(Li^+ + RE^{3+})/Nb$ ratio ($RE^{3+} = Er^{3+} + Yb^{3+}$ or Yb^{3+}) in two V1 crystals, which do not precipitate, was roughly evaluated by using the OAE data obtained. The results are shown in table 1. It is worth noting that the $(Li^+ + RE^{3+})/Nb$ ratio in the as-grown crystals is about 93.8%. The V1 procedure results in an increase in the $(Li^+ + RE^{3+})/Nb$ ratio up to 98.1 and 97.7% for the doubly and singly doped crystals, respectively. For three precipitated VTE crystals, because the generated precipitates result in a substantial

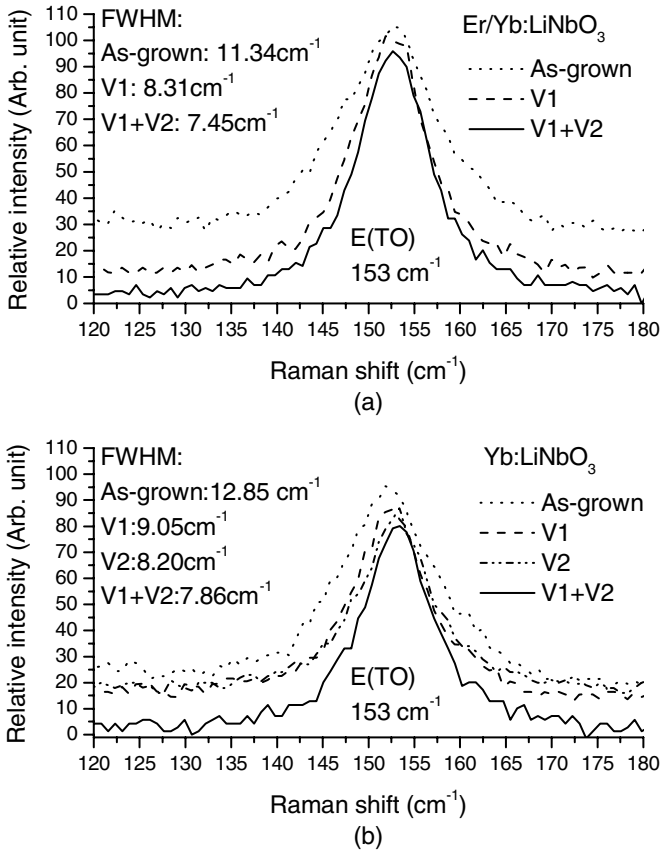

Figure 6. E(TO)-153 cm^{-1} Raman phonons in (a) as-grown, V1 and V1 + V2 Er/Yb:$LiNbO_3$ crystals and (b) as-grown, V1, V2 and V1 + V2 Yb:$LiNbO_3$ crystals. The FWHM of the phonon is indicated for each crystal.

OAE redshift, equation (2) is no longer suitable for these crystals. We should consider other methods. As an alternative method, the relation of the crystal composition to Raman linewidth of the 153 cm^{-1} E phonon is used for a rough estimation of the ($Li^+ + RE^{3+}$) content in the three precipitated crystals. Taking rare-earth doping effect into account (the rare-earth doping induces the broadening of the Raman linwidth), the original experiential formula, which is suitable for evaluation of the composition in a pure crystal [24], can be modified as follows:

$$y = C - 0.26834\Gamma, \tag{3}$$

where y is the $RE^{3+} + Li^+$ content and Γ is the linewidth of the 153 cm^{-1} E(TO) Raman phonon; C depends on the doping level and can be determined by using the y and Γ values of the corresponding as-grown crystal. Figure 6 shows the 153 cm^{-1} E(TO) Raman phonon in all the as-grown and VTE-treated crystals studied here. One can see that VTE treatment induces an obvious narrowing of the phonon linewidth whether the crystal is with or without the precipitates. The full-width at half-maximum (FWHM) was evaluated and collected in figure 6 and table 1. The ($Li^+ + RE^{3+}$)/Nb ratios in both unprecipitated and precipitated crystals are evaluated according to equation (3). The results are listed in table 1 in comparison with those obtained from the OAE. We note from table 1 that, for the two V1 crystals, the Raman results

are in good agreement with the OAE data, showing that the data yielded by the two methods seem to be reliable. It can also be concluded from the $(Li^+ + RE^{3+})/Nb$ ratios shown in table 1 that the VTE procedure has brought all the congruent crystals towards stoichiometric composition. The $(Li^+ + RE^{3+})/Nb$ ratio increases as the VTE strength increases.

Next, let us further discuss the effect of the VTE treatment on absorptions with respect to the electronic transitions of Er^{3+} and Yb^{3+}. Table 1 summarizes some optical absorption parameters including peak position and FWHM of two typical absorption peaks at 980 and 1530 nm, which involve the $^2F_{7/2} \rightarrow {}^2F_{5/2}$ (Yb^{3+}), $^4I_{15/2} \rightarrow {}^4I_{11/2}$ (Er^{3+}) and $^4I_{15/2} \rightarrow {}^4I_{13/2}$ (Er^{3+}) transitions. The absorption coefficient integral over the whole band concerned with these transitions are also shown in table 1. For the unprecipitated Er/Yb crystal, i.e. the Er/Yb crystal with V1 procedure, the effect of the VTE treatment is negligible. As one proceeds from the as-grown crystal to the V1 crystal, no substantial spectral alteration is observed except for very slight redshift (less than 0.5 nm) of the absorption peaks at 1530 nm, about 10% narrowing of the 1530 nm peak and about 10% reduction of the integrated absorption coefficient of the 1450–1650 nm band. Peak redshift and integrated absorption coefficient reduction also appear in the 880–1050 nm region as shown in the inset to figure 2. But the FWHM of the 980 nm peak becomes broad by a factor of 10% as shown by the FWHM data listed in table 1. Similar absorption features in the 880–1050 nm region are also observed for the V1 Yb:$LiNbO_3$ crystal as shown in the inset to figure 5 and the data listed in table 1.

Significant spectral features with respect to the Er^{3+} absorptions are observed for the precipitated Er/Yb codoped crystal. The features are especially evident in the 1450–1650 nm region. In figure 3(a), the most evident feature is the significant enhancement of the 1480 nm absorption band. Meanwhile, four weak peak components at 1474, 1478, 1483 and 1487 nm superpose upon this enhanced band, and several additional absorption peaks near 1497, 1503, 1519 and 1536 nm are resolved. Similar to the unprecipitated Er/Yb crystal, the 1530 nm absorption peak of the precipitated Er/Yb crystal also shows a slight redshift in peak position, a slight narrowing of FWHM and a slight reduction of the integrated absorption coefficient. Reduction of the integrated absorption coefficient also takes place in other bands, such as the bands around 380 and 980 nm. In addition to the remarkable reduction of the absorption coefficient area, the absorption band around 380 nm ($^4I_{15/2} \rightarrow {}^4G_{11/2}$) displays another interesting feature: the original 380 nm band of the as-grown crystal splits into two components located at 379 and 381 nm. In the 880–1050 nm region, in addition to the remarkable reduction of the integrated absorption coefficient (by ≈50%), the precipitated Er/Yb crystal also shows slight redshift of the 980 nm peak position and broadening of the peaks at 918, 955 and 980 nm in comparison with the as-grown crystal. Similar spectral features are also obvious in the spectra of the two precipitated singly Yb-doped crystals as shown in figure 5. In addition to the opacity, significant reduction of the absorption in the 880–1050 nm region and broadening of the component peaks, the appearance of an additional weak peak at 972 nm (see figure 5) is another important optical absorption feature that characterizes the precipitation of the Yb:$LiNbO_3$ crystal. To further verify this additional absorption, absorption measurement has been performed also on the thermally calcined $YbNbO_4$ powder. Unfortunately, it is very difficult to resolve such a weak absorption near 972 nm because of very poor signal-to-noise ratio.

Finally, figure 7 shows the OH^- absorption spectra of the as-grown and VTE-treated Er/Yb codoped and singly Yb-doped crystals. One can see that the VTE treatment results in a significant reduction of the OH absorption. The reduction increases as the VTE is strengthened. For the two V1 + V2 crystals, the OH^- contained in the crystals is essentially removed. This OH^- spectral characteristic is similar to the case of the singly Er-doped $LiNbO_3$ crystal [19].

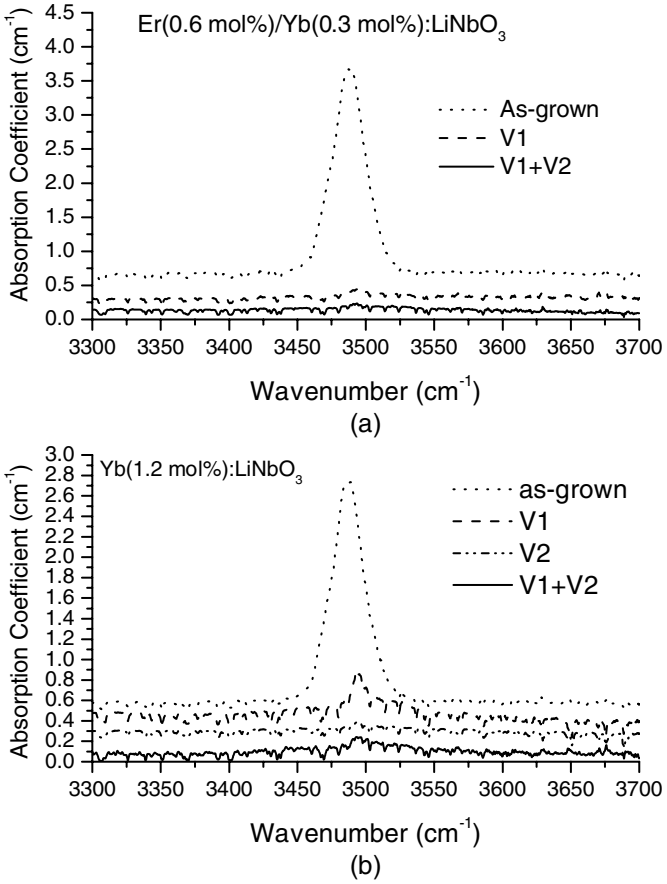

Figure 7. OH^- absorption spectra of (a) as-grown and VTE-treated Er/Yb codoped $LiNbO_3$ crystals and (b) as-grown and VTE-treated singly Yb-doped (1.2 mol%) $LiNbO_3$ crystals.

3.2. X-ray diffraction results and determination of the precipitation phase

In this section, we try to determine the precipitated phases in Er/Yb:$LiNbO_3$ and Yb:$LiNbO_3$ crystals through combined optical absorption characteristics and x-ray powder diffraction patterns of these precipitated crystals. Figure 8 shows the x-ray powder diffraction patterns of several selected crystals with the precipitates. The patterns b, c and d correspond to the V1 + V2 Yb:$LiNbO_3$, V2 Yb:$LiNbO_3$ and V1 + V2 Er/Yb:$LiNbO_3$, respectively. For convenience, let us, firstly, consider the precipitates generated in the Yb:$LiNbO_3$ crystals. Figure 8(a) also shows the diffraction pattern of the thermally calcined $YbNbO_4$ powder. A careful comparison has shown that the diffraction data of the calcined powder are essentially consistent with results of the powder diffraction files (PDF) 23-1480 (measured data) and 81-1976 (calculated results) provided by the Joint Committee on Powder Diffraction Standards (JCPDS). In figure 8(a), the strongest diffraction peaks appear at the 2θ angles of 28.80 and 30.44°, which correspond to the d-values of 2.9341 and 3.0974 Å, respectively. In figure 8(b), two additional weak and broad peaks are resolved around the 2θ angle 30° in comparison with the diffraction pattern of the $LiNbO_3$ phase. Further examining their diffraction data have revealed that the two additional peaks, located at 28.84 and 30.38° with the respective d-values of 3.0932

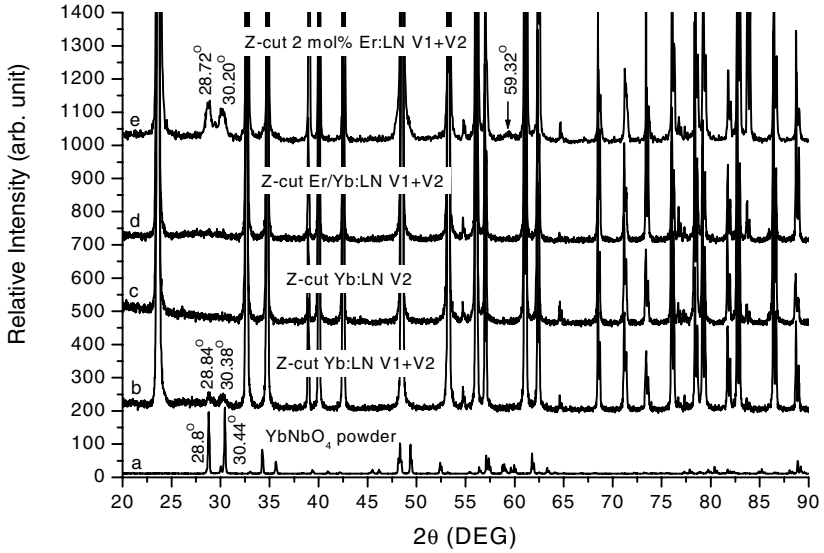

Figure 8. X-ray powder diffraction patterns of thermally calcined $YbNbO_4$ powder (a), Yb:$LiNbO_3$ with the VTE procedures of V1 + V2 (b), Yb:$LiNbO_3$ with the V2 procedure (c), Er/Yb:$LiNbO_3$ with the V2 + V3 procedures (d) and *Z*-cut Er(2.0 mol%):$LiNbO_3$ with the V2 + V3 procedures (e). Weak and broad peaks around 2θ angles of 30 or 59° are the characteristic diffractions with respect to $ErNbO_4$ or $YbNbO_4$ phase.

and 2.9398 Å, correspond well to the above *d*-values of the two strongest diffractions of the thermally calcined $YbNbO_4$ powder. This well-corresponding relation implies that the precipitation phase induced by VTE treatment in Yb:$LiNbO_3$ may be $YbNbO_4$. Since the two strongest peaks of $YbNbO_4$ are already very weak in figure 8(b), the other medium-intensity or weak peaks of $YbNbO_4$ shown in figure 8(a) must be weaker in figure 8(b). It can be anticipated that, with the exception of the two strongest peaks, the other very weak diffraction peaks of $YbNbO_4$ may either hide under the corresponding peaks belonging to $LiNbO_3$ or be buried by the background noise and hence are indiscernible. It should be pointed out that the precipitate $ErNbO_4$ induced by VTE treatment in an *X*-cut or *Z*-cut singly Er-doped (2.0 mol%) $LiNbO_3$ crystal is characterized not only by two similar strong peaks located around 30°, but also by two additional weak and broad diffraction peaks located around 30 and 59° [21]. As an example, in figure 8(e), we show the case of a Z-cut 2.0 mol% Er:$LiNbO_3$ crystal, which has the same VTE procedures as the V1 + V2 Er/Yb:$LiNbO_3$ and Yb:$LiNbO_3$. The four discernible characteristic peaks belonging to $ErNbO_4$ are located around 28.72, 29.42, 30.20 and 59.32°. The more characteristic diffractions discernible in the x-ray diffraction pattern of VTE Er:$LiNbO_3$ crystal are due to higher concentration of the $ErNbO_4$ precipitates (2.0 mol% Er-doping!). Fewer characteristic diffractions being discernible in the pattern of the V1 + V2 Yb:$LiNbO_3$ crystal may be attributed to the relatively lower doping level of Yb, 1.2 mol%.

Next, we turn to the diffraction pattern c shown in figure 8. This pattern corresponds to the V2 Yb:$LiNbO_3$ crystal that experienced a weak VTE strength relative to the V1 + V2 crystal. The two characteristic diffractions observed in figure 8(b) cannot be resolved. We attribute the characteristic diffractions of $YbNbO_4$ indiscernible in figure 8(c) to a lower extent of precipitation induced by the weaker VTE strength. The lower extent of precipitation in the V2 Yb:$LiNbO_3$ crystal in comparison with the V1 + V2 crystal can be seen from their absorption characteristics. In figure 4, the transparency of the V2 sample is obviously better

than that of the V1 + V2 sample. In figure 5, the 972 nm characteristic absorption peak of the $YbNbO_4$ phase in the V2 sample is found to be weaker somewhat when compared with the V1 + V2 sample. Moreover, the decrease in the integrated absorption coefficient in the range of 880–1050 nm is obviously more serious for the V1 + V2 sample as shown by the data listed in table 1.

The determination of the precipitation phase in the V1 + V2 Er/Yb codoped crystal is complicated somewhat because of the simultaneous presence of two kinds of rare-earth ions in the crystal. It can be anticipated that the precipitate in the crystal may be $ErNbO_4$ or $YbNbO_4$ or both of them. Unfortunately, the characteristic x-ray diffractions belonging to $ErNbO_4$ are not discernible as shown in figure 8(d). This is also because of the lower doping level of the total rare-earth ion doping level (only 0.9 mol%!). Thus, the precipitation phase in this crystal is determined only with the aid of its optical absorption characteristics. We now return to figure 3(a). The significant absorption characteristics of the V1 + V2 Er/Yb codoped crystal result from the $ErNbO_4$ phase. This argument can be clarified on the basis of our earlier work [19, 25]. For convenience, in figure 3(b), we show a comparison of the absorptions in thermally calcined $ErNbO_4$ powder and as-grown and (V1 + V2)-treated singly Er-doped (2.0 mol%) crystals, in which the presence of the $ErNbO_4$ phase has been confirmed by the x-ray diffraction pattern shown in figure 8(e). One can see that the absorption spectrum of the V1 + V2 Er/Yb:$LiNbO_3$ crystal shown in figure 3(a) is in good agreement with the spectra of thermally calcined $ErNbO_4$ powder and VTE-treated crystal with unpolished surfaces shown in figure 3(b), especially in the wavelength region below 1540 nm. It can be thus concluded that the precipitates generated in the V1 + V2 Er/Yb codoped crystal contain the $ErNbO_4$ phase. Next, we consider the possibility of precipitates containing the $YbNbO_4$ phase. As shown in figure 8(d), the x-ray pattern also fails to display the characteristic diffraction peaks with respect to $YbNbO_4$. Again, we only repose the confidence in the optical absorption characteristics. As mentioned above, the characteristic absorption peak of $YbNbO_4$ is the appearance of an additional weak peak at 972 nm. In connection with the spectrum of the V1 + V2 Er/Yb:$LiNbO_3$ shown in figure 2, such an absorption peak is indiscernible (for convenience, the 972 nm position is marked in figure 2 by an arrow). Nevertheless, we cannot rule out the possibility that the precipitates contain the $YbNbO_4$ phase because the doping level of Yb in the codoped crystal is only 0.3 mol%, which is four times less than the x-ray diffraction and optical absorption detectable doping level, 1.2 mol% in the case of Yb:$LiNbO_3$. Such a low doping level corresponds to a low $YbNbO_4$ precipitate concentration. Moreover, as the 972 nm absorption in the 1.2 mol% Yb:$LiNbO_3$ is already very weak, it should be weaker in the codoped crystal with only 0.3 mol% Yb^{3+} doping. Thus, it is comprehensive that both x-ray diffraction and optical absorption are insensitive to the characteristic x-ray diffractions around the 2θ angle of 30° and characteristic optical absorption near 972 nm. In addition, the absorption with respect to the $^4I_{15/2} \rightarrow {}^4I_{11/2}$ transition of Er^{3+} just overlaps in this region. The spectral mixing increases the complexity. Thus, we cannot simply exclude the presence of $YbNbO_4$ on the basis of the present experimental data. In conclusion, the precipitated Er/Yb:$LiNbO_3$ crystal definitely contains the $ErNbO_4$ phase. But the possibility that the crystal simultaneously contains the $YbNbO_4$ phase cannot be ruled out. So we call the precipitation phase in the codoped crystal as the $ErNbO_4$ (+$YbNbO_4$).

3.3. Crystallographic morphology of $ErNbO_4$ and $YbNbO_4$ precipitates

Along with determination of the precipitation phase, we turn to the crystallography and morphology of the $ErNbO_4$ or $YbNbO_4$ precipitates. According to the powder diffraction files 22-1095 (for $ErNbO_4$, measured data), 23-1480 (for $YbNbO_4$, measured data) and

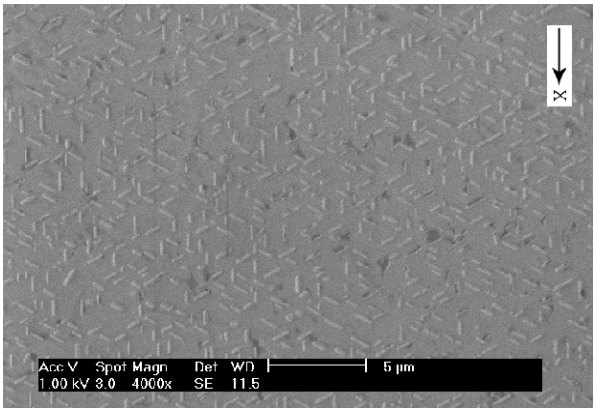

Figure 9. SEM images of precipitates grown on the surface of a VTE-treated (V1 + V2) Er/Yb:$LiNbO_3$ crystal with an image amplification of 4000×.

81-1976 (for $YbNbO_4$, calculated result), both phases have a similar crystallography. Both belong to the monoclinic system and have the same crystal structure (fergusonite-like structure) with the space group I2 (5th space group in the list of total 230 members). Every unit cell contains four molecular formulae. The lattice constants are $a = 5.279$ Å, $b = 10.91$ Å, $c = 5.064$ Å and $\beta = 94.32^\circ$ for $ErNbO_4$ and $a = 5.231$ Å, $b = 10.83$ Å, $c = 5.038$ Å and $\beta = 94.25^\circ$ for $YbNbO_4$.

Figures 9 and 10 show SEM images taken from the surfaces of V1 + V2 Er/Yb codoped and singly Yb-doped crystals, respectively. Figure 9 corresponds to an image magnification of 4000×. In figure 10, images a, b, c and d correspond to an image magnification of 2000×, 4000×, 8000× and 16000×, respectively. The direction of the crystallographic axis X of the substrate is marked on each image. We note that some $ErNbO_4$ or $YbNbO_4$ precipitates are clearly observed on the surfaces of the two substrates. We can see from figure 9 that the precipitate in the (0001) crystallographic plane is regular and seems to be rod-like. It can be further seen that these precipitates have only three different orientations. It is more interesting that these orientations make an approximately same angle of 60 or 120° to each other. Such an intersecting angle is just consistent with the angle between the crystallographic axes of the $LiNbO_3$ crystal lying in the (0001) plane. Moreover, the three orientations are nearly parallel to the three crystallographic axes lying in the (0001) plane of the $LiNbO_3$ crystal. A similar crystallographic morphology was also observed for the $ErNbO_4$ precipitates that grow on the surface of the VTE-treated singly Er-doped $LiNbO_3$ crystals [26]. Three-dimensional crystallographic morphology of the precipitates has been tentatively anticipated in that work by combining the effect of cut of the substrate. The precipitate is actually not rod-like. It grows, to a larger extent, in a flat polyhedron-like crystallographic morphology. In fact, individual crystallographic planes are discernible for some $YbNbO_4$ precipitates shown in images c and d in figure 10. The planar dimension of the polyhedron-like precipitates in the (0001) plane is roughly evaluated and listed in table 1. For the codoped crystal, the precipitates have an approximate length range of 200–980 nm and an approximate width range of 100–285 nm.

A similar crystallographic morphology is also observed for the $YbNbO_4$ precipitates as shown in figure 10. The only difference from the precipitates shown in figure 9 is in the dimension. One can see from table 1 that the $YbNbO_4$ precipitates have a rough length range of 400–1030 nm and a rough width range of 250–630 nm. From the viewpoint of mean dimension,

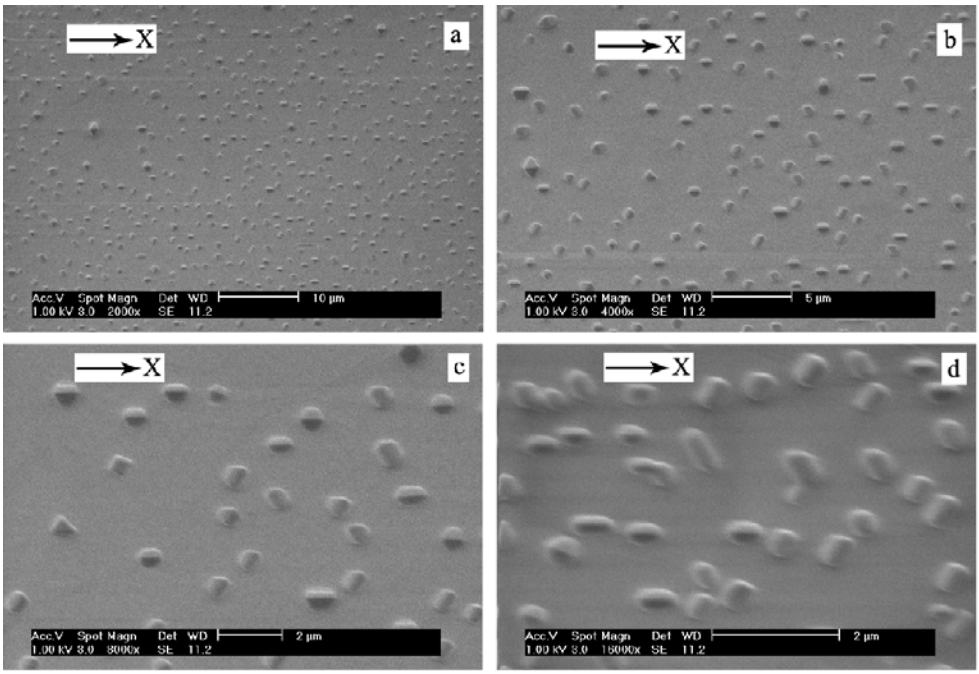

Figure 10. SEM images of precipitates grown on the surface of a (V1 + V2)-treated Yb:$LiNbO_3$ crystal with an image amplification of 2000× (a), 4000× (b), 8000× (c) and 16000× (d), respectively.

the $YbNbO_4$ precipitates are shorter and thicker than the precipitates grown on the surface of the Er/Yb codoped crystal as shown by the images in figures 9 and 10(b), which have the same image magnification of 4000×. In comparison with the $ErNbO_4$ precipitates grown in singly Er-doped crystals, the size of the precipitates here is small. For the case of singly Er-doping, the rough three-dimensional size is in the magnitude of sub-μm × μm × μm and the longest length in the (0001) plane reaches 10 μm [26]. It is obvious that all of the above size differences result from the difference in the rare-earth doping level. Under the same VTE condition, a lower doping level corresponds to a smaller size of the precipitates and a higher doping level corresponds to a larger size of the precipitates.

The roughness of the surface on which the precipitates grew was characterized by using an atomic force microscope (AFM). The characterization was performed on three pieces of (V1 + V2)-treated Yb(Er):$LiNbO_3$ crystals, including two Er/Yb codoped crystals with and without the surface polishing process and one piece of singly Yb-doped crystal without surface polishing. Images similar to those shown in figures 9 and 10 were observed on the surfaces of the two unpolished crystals, but not on the surface of the polished one. The rms roughness is 30 nm for the unpolished Er/Yb codoped crystal, 31.8 nm for the unpolished singly Yb-doped crystal and 0.63 nm for the polished crystal.

3.4. Precipitates in the bulk crystal

It should be pointed out that all the above-mentioned experimental results obtained from optical absorption, Raman scattering and SEM characterizations are limited to those VTE-treated

crystals that were not subjected to a polishing process after the VTE procedure. The powder sample used for x-ray powder diffraction measurement was also powdered from the as-VTE-treated crystals. The above SEM results confirm that the precipitates grow on the surface of the substrate. Then, one may ask what is happening in the bulk crystal, if similar precipitates were also induced in the bulk. This can be readily examined by simply polishing the two surfaces of the sample and then repeating the optical absorption measurements. We selected a piece of (V1 + V2)-treated *Z*-cut Er/Yb:$LiNbO_3$ crystal and carried out the polishing process. The polish was performed on the two main surfaces (i.e. *Z*-planes). The sample thickness was reduced from the original 0.94 to 0.68 mm, sufficiently guaranteeing that the precipitates grown on the two main surfaces have been completely removed. (This is confirmed by the subsequent AFM checking as mentioned above.) It was found that the crystal after the fine-polish process is still opaque, showing that the precipitates also exist in the bulk. The subsequent optical absorption measurement was carried out on this polished crystal. Indeed, a nearly identical absorption curve as the solid plot shown in figure 1 was obtained (the curve is therefore not shown in figure 1). The absorption spectrum of the polished sample in the 1450–1650 nm region is shown in figure 3(a) (see the filled-block-marked curve). One can see that similar characteristic absorptions associated with the $ErNbO_4$ precipitates are observed. The same experimental result was also obtained for the VTE-treated singly Er-doped (2.0 mol%) $LiNbO_3$ crystal. In figure 3(b), we additionally show the absorption spectrum of one piece of (V1 + V2)-treated singly Er-doped (2.0 mol%) crystal with two polished surfaces. To guarantee that the precipitates grown on the two surfaces were removed completely, the thickness of the crystal was reduced to 0.71 mm from the original 1 mm. One can see that the absorption characteristics of the $ErNbO_4$ phase are still evident. It can be thus concluded that the precipitates grow not only on the surface but also in the bulk.

4. Conclusion

The VTE treatment has brought all Er/Yb codoped and singly Yb-doped $LiNbO_3$ crystals towards stoichiometric composition. Accompanying this behaviour, a relatively strong VTE treatment results in the formation of submicron-size $ErNbO_4$ (+$YbNbO_4$) and $YbNbO_4$ flat polyhedron-like precipitates in the Er/Yb:$LiNbO_3$ crystals and Yb:$LiNbO_3$, respectively. On the other hand, a relatively weak VTE procedure cannot induce the precipitation of these singly or doubly doped crystals. The characteristics of optical absorption, crystalline structure and crystallographic morphology of the precipitates in the Er/Yb:$LiNbO_3$ crystal are similar to the case of singly Er-doping reported earlier. Because of the lower rare-earth doping level and hence the lower content of the precipitates in the crystal, the x-ray diffraction fails to resolve the characteristic diffractions with respect to the precipitation phase in the Er/Yb:$LiNbO_3$. Nevertheless, the optical absorption characteristics are enough to conclude that the $ErNbO_4$ phase dominates the precipitates generated in the Er/Yb crystal. Because of the lower doping level of the Yb^{3+} relative to the codopant Er^{3+}, the $YbNbO_4$ content in the codoped crystal may be too low to be sensitive to both the optical absorption and x-ray diffraction. In this sense, the possibility of the precipitates containing the $YbNbO_4$ phase cannot be unambiguously excluded on the basis of the present experimental results.

Similar to the case of the $ErNbO_4$ precipitate generated in the singly Er-doped $LiNbO_3$, the $YbNbO_4$ precipitate generated in the Yb:$LiNbO_3$ crystal was also characterized mainly by two x-ray diffractions around the 2θ angle 30°. Its characteristic optical absorption is the appearance of an additional weak absorption near 972 nm. The presence of the $YbNbO_4$ precipitates in the host matrix also results in the opacity due to their Rayleigh scattering, the considerable broadening of two main absorption peaks near 955 and 980 nm, and the

reduction of the whole band absorption with respect to the electronic transition of Yb^{3+}. The $YbNbO_4$ precipitate has the same space group I2, a very close lattice constant and similar crystallographic morphology as the $ErNbO_4$ precipitate. The $ErNbO_4$ or $YbNbO_4$ precipitate grows mainly along the crystallographic axes lying in the plane perpendicular to the optical axis of the substrate. The size of the precipitate depends on the doping level and the VTE condition. Additional optical absorption measurements on the precipitated crystal with polished surfaces have shown that similar precipitates also exist in the bulk crystal.

In addition to the spectral, structural and morphological characteristics mentioned above, the VTE-treated Er/Yb codoped or singly Yb-doped $LiNbO_3$ crystals also reveal other absorption features similar to those of VTE-treated Er:$LiNbO_3$ crystals. For the unprecipitated crystal, the VTE treatment results in considerable blueshift of the optical absorption edge, a slight increase in the transmittance of the crystal and a slight broadening of the main absorptions at 955 and 980 nm with respect to Yb^{3+}. For a VTE crystal, with or without the precipitates, VTE treatment results in slight redshift and narrowing of the 1530 nm absorption peak, reduction of the whole band absorption in the 1450–1650 nm region for Er^{3+} and the 880–1050 nm region for $Yb^{3+} + Er^{3+}$ ions and significant reduction or even complete removal of the OH^- content in the crystal.

The present results can offer considerable guidance to the realization of nearly stoichiometric Er(/Yb):$LiNbO_3$-based active waveguide devices in the future. Overall consideration of all other singly Er-doped VTE crystals allows us to conclude that the total doping level of the rare-earth ions, 0.9 mol% in the Er/Yb codoped crystal and 1.2 mol% in the Yb:$LiNbO_3$ crystal, just lies in the proximity of a critical doping level (around 1.0 mol%), beyond which the VTE treatment results in formation of precipitates in the substrate. A total doping level below 0.9 mol% is thus proposed. Below this doping level, the VTE treatment not only cannot induce the formation of precipitates within the usual VTE strength 1100 °C/100 h, but also allows improvement of some spectral and spectroscopic properties as described above. These improved spectral and spectroscopic properties plus several intrinsic advantages of a pure nearly stoichiometric $LiNbO_3$ crystal over the congruent material, such as lower substrate refractive index, one order of magnitude lowering of the coercive field strength for PPLN as well as exciting photorefractive properties [27, 28], suggest potential uses of a nearly stoichiometric Er(/Yb):$LiNbO_3$ for active waveguide devices.

References

[1] Brinkmann R, Sohler W and Suche H 1991 *Electron. Lett.* **27** 415
[2] Becker Ch *et al* 2000 *IEEE J. Sel. Top. Quantum Electron.* **6** 101
[3] Sohler W and Suche H 1999 *Integrated Optical Circuits and Components: Design and Application* ed E J Murphy (New York: Dekker) pp 127–59
[4] Amin J, Aust J A and Sanford N A 1996 *Appl. Phys. Lett.* **69** 3785
[5] Helmfrid S, Arvidsson G, Webjorn J, Linnarsson M and Pihl T 1991 *Electron. Lett.* **27** 913
[6] Huang C H and McCaughan L 1996 *IEEE J. Sel. Top. Quantum Electron.* **2** 367
[7] Das B K, Ricken R and Sohler W 2003 *Appl. Phys. Lett.* **83** 1514
[8] Das B K, Ricken R, Quiring V, Suche H and Sohler W 2004 *Opt. Lett.* **29** 165
[9] Schreiber G, Hofmann D, Grundkotter W, Lee Y L, Suche H, Quiring V, Ricken R and Sohler W 2001 *Proc. SPIE* **4277** 144
[10] Huang C H and McCaughan L 1997 *IEEE Photon. Technol. Lett.* **9** 599
[11] Lifante G, Cantelar E, Munoz J A, Nevado R, Sanz-Garcia J A and Cusso F 1999 *Opt. Mater.* **13** 181
[12] Cantelar E, Munoz J A, Sanz-Garcia J A and Cusso F 1998 *J. Phys.: Condens. Matter* **10** 8893
[13] Cantelar E and Cusso F 1999 *Appl. Phys. B: Laser Opt.* **69** 29
[14] Cantelar E, Nevado R, Martin G, Sanz-Garcia J A, Lifante G, Cusso F, Hernandez M J and Permas P L 2000 *J. Lumin.* **87–89** 1096
[15] Amin J, Aust J A, Veasey D L and Sanford N A 1998 *Electron. Lett.* **34** 456

[16] Cantelar E, Torchia G A, Sanz-Garcia J A, Permas P L, Lifante G and Cusso F 2003 *Appl. Phys. Lett.* **83** 2991
[17] Gill D M, McCaughan L and Wright J C 1996 *Phys. Rev.* B **53** 2334
[18] Zhang D L, Chen X J, Wang Y F, Zhu D S, Wu B and Lan G X 2002 *J. Phys. Chem. Solids* **63** 345
[19] Zhang D L, Pun E Y B, Chen X J, Wang Y, Jin Y H, Zhu D S and Wu Z K 2002 *J. Appl. Phys.* **91** 4014
[20] Zhang D L and Pun E Y B 2003 *J. Appl. Phys.* **93** 3141
[21] Zhang D L, Lan G X, Chen X J and Zhu D S 2002 *Appl. Phys. A: Mater. Sci. Process.* **74** 265
[22] Zhang D L and Pun E Y B 2003 *J. Appl. Phys.* **94** 1178
[23] Wohlecke M, Corradi G and Betzler K 1996 *Appl. Phys. B: Laser Opt.* **63** 323
[24] Malovichko G I, Grachev V G, Kokanyan E P, Schirmer O F, Betzler K, Gather B, Jermann F, Klauer S, Schlarb U and Wohlecke M 1993 *Appl. Phys. A: Solids Surf.* **56** 103
[25] Zhang D L, Wang Y F, Yu Y Z, Chen C H, Yao J Q and Pun E Y B 2004 *Opt. Mater.* **25** 379
[26] Zhang D L, Wong W H and Pun E Y B 2004 *J. Cryst. Growth* **271** 184
[27] Furukawa Y, Kitamura K and Takekawa S 1998 *Opt. Lett.* **23** 1892
[28] Furukawa Y, Kitamura K, Takekawa S, Miyamoto A, Terao M and Suda N 2000 *Appl. Phys. Lett.* **77** 2494